Available online at www.sciencedirect.com
ScienceDirect
Journal of Solid State Chemistry 180 (2007) 1775–1782
JOURNAL OF SOLID STATE CHEMISTRY
www.elsevier.com/locate/jssc

Synthesis of layered cathode material $Li[Co_xMn_{1-x}]O_2$ from layered double hydroxides precursors

Yanluo Lu[a], Min Wei[a,*], Lan Yang[a], Congju Li[b,**]

[a]State Key Laboratory of Chemical Resource Engineering, Beijing University of Chemical Technology, Beijing 100029, PR China
[b]Beijing Key Laboratory, Beijing Institute of Clothing Technology, Beijing 100029, PR China

Received 26 December 2006; received in revised form 24 March 2007; accepted 1 April 2007
Available online 6 April 2007

Abstract

Cathode materials $Li[Co_xMn_{1-x}]O_2$ for lithium secondary batteries have been prepared by a new route—precursor method of layered double hydroxides (LDHs). *In situ* high-temperature X-ray diffraction (HT-XRD) and thermogravimetric analysis coupled with mass spectrometry (TG–MS) were used to monitor the structural transformation during the reaction of CoMn LDHs and $LiOH \cdot H_2O$: firstly the layered structure of LDHs transformed to an intermediate phase with spinel structure; then the distortion of the structure occurred with the intercalation of Li^+ into the lattice, resulting in the formation of layered $Li[Co_xMn_{1-x}]O_2$ with α-$NaFeO_2$ structure. Extended X-ray absorption fine structure (EXAFS) data showed that the Co–O bonding length and the coordination number of Co were close to those of Mn in $Li[Co_xMn_{1-x}]O_2$, which indicates that the local environments of the transitional metals are rather similar. X-ray photoelectron spectroscopy (XPS) was used to measure the oxidation state of Co and Mn. The influences of Co/Mn ratio on both the structure and electrochemical property of $Li[Co_xMn_{1-x}]O_2$ have been investigated by XRD and electrochemical tests. It has been found that the products synthesized by the precursor method demonstrated a rather stable cycling behavior, with a reversible capacity of 122.5 mAh g^{-1} for the layered material $Li[Co_{0.80}Mn_{0.20}]O_2$.
© 2007 Published by Elsevier Inc.

Keywords: Layered $Li[Co_xMn_{1-x}]O_2$; LDHs; Precursor method; Cathode materials; *In situ* HT-XRD

1. Introduction

There is much interest in lithium manganese oxides for use as cathode materials for advanced lithium secondary batteries to replace the expensive and relatively low capacity lithium cobalt oxide system [1–6]. Layered lithium manganese oxides have been prepared using hydrothermal methods [1] and ion-exchange methods [4,6]. They however tend to convert to spinel-like structures on cycling, which is facilitated by the oxygen cubic-close-packing found in both lattices [2–4]. Recently, extensive attention has been paid to the layered $LiNi_xMn_{1-x}O_2$ and $LiCo_xMn_{1-x}O_2$ compounds, in terms of its low cost, high discharge capacity, long cycling stability and thermal safety [7–9]. Several solid reaction method [10–13] and sol–gel synthesis method [14] have been used to prepare $LiCo_xMn_{1-x}O_2$, but stacking faults and significant capacity fading on cycling of these materials occurred during cycling. As a result, some efforts were reported to improve the electrochemical properties of $LiM_xMn_{1-x}O_2$ such as coated with $Al(OH)_3$ [15] and doping a small part of Co or Ni [16,17].

Layered double hydroxides (LDHs) [18,19] have been known for a considerable time and have been widely studied. The basic layer structure of LDHs is based on that of brucite $[Mg(OH)_2]$ with the CdI_2 type, which consists of magnesium ions surrounded approximately octahedrally by hydroxide ions. These octahedral units form infinite layers by edge sharing, with the hydroxide ions sitting perpendicular to the plane of the layers. The layers then stack on top of one another to form the tree-dimensional structure. The basic structure of an LDH may be derived by substitution of a fraction of the divalent cations in a brucite lattice by trivalent cations such that the layers

*Corresponding author. Fax: +86 010 64425385.
**Also to be corresponded to.
E-mail addresses: weimin@mail.buct.edu.cn (M. Wei), clycongjuli@bict.edu.cn (C. Li).

0022-4596/$ - see front matter © 2007 Published by Elsevier Inc.
doi:10.1016/j.jssc.2007.04.001

acquire a positive charge, which is balanced by intercalation of anions between the layers [20]. LDHs may be described by the general formula $[M^{II}_{1-x}M^{III}_{x}(OH)_2]^{x+}[A^{n-}_{x/n}\cdot yH_2O]^{x-}$, where M^{II} and M^{III} are divalent and trivalent metal cations, A^{n-} is an $-n$ valent anion. It is often said that pure LDH phases can commonly be formed for stoichiometries in the range $0.20<x<0.33$ [21–24], i.e., M^{II}/M^{III} ratios in the range 2–4. In the hydrotalcite-like compounds [19,25–28], the M^{II}/M^{III} isomorphous substitution in octahedral sites of the hydroxide sheet results in a well-distributed single phase by coprecipitation method.

In the present work, the layered $Li[Co_xMn_{1-x}]O_2$ materials were prepared by the precursor method of LDHs. Firstly, the precursor CoMn LDHs was synthesized by coprecipitation, then it was mixed with appropriate amount of $LiOH\cdot H_2O$ sufficiently and calcined in air at 900 °C. Layered $Li[Co_xMn_{1-x}]O_2$ materials with α-$NaFeO_2$ type structure were obtained. The structure and the initial electrochemical performance of the products have been examined.

2. Experimental

CoMn LDHs with Co/Mn molar ratio 2, 3 and 4, respectively, were prepared by coprecipitation method similar to MgAl LDHs described previously [29]. A solution containing the metallic nitrate salts $Co(NO_3)_2\cdot 6H_2O$ and $Mn(NO_3)_2$ (0.6 M) with a definite molar ratio was delivered into a beaker at room temperature. A second aqueous solution containing 100 mL NaOH (1 M) and Na_2CO_3 (0.5 M) was added dropwise over 3 h into the metallic nitrate salts solution with vigorous stirring. Air was bubbled throughout the reaction mixture during the entire addition period, and thus most Mn^{II} was oxidized to Mn^{III} by oxygen in air. As a result, M^{II}/M^{III} molar ratio in LDHs is approximately in accordance with Co/Mn ratio. The resulting suspension was aged at room temperature for 12 h, and the precipitation obtained was collected by centrifugation, washed thoroughly with distilled water. Then it was mixed with appropriate amount of $LiOH\cdot H_2O$ (Li/(Co + Mn) = 1.1) sufficiently by grinding, and dried at 70 °C for 12 h. The mixture was calcined at 900 °C for 24 h in air and cooled to room temperature. The product was washed with distilled water thoroughly and dried at 70 °C for 12 h in air.

In situ high-temperature X-ray diffraction (HT-XRD) measurements were carried out in the 30–900 °C temperature range for the mixture of CoMn LDHs (Co/Mn = 2/1) and $LiOH\cdot H_2O$ by using a D/MAX2500VB2+/PC diffractometer (using Cu*K*α radiation and graphite monochromator) with the following conditions of sequential temperature increase (10 °C/min) and of temperature holding time (5 min) before measurement. The XRD data of $Li[Co_xMn_{1-x}]O_2$ were collected from $2\theta = 10^\circ$ to $2\theta = 85^\circ$ with 0.04° steps and 10 s per step. Unit cell parameters were obtained by least square refinement of the powder XRD data. TG-MS measurement was carried out on a Pyris Diamond TG/DTA instrument (Perkin Elmer instruments) equipped with a mass spectrometer (Thermo-Star TM) under N_2 atmosphere. The temperature-programmed rate was 10 °C/min, in the measured temperature range 30–800 °C. Gaseous emission was analyzed at intervals of 1 s. Extended X-ray absorption fine structure (EXAFS) data were collected at the Beijing Synchrotron Radiation Facility and analyzed with the Crius2 XAFS program (Daresbary). Raw spectra were Fourier transformed to *R* space. The atomic distance *R* and the coordination number (CN) of the sample were calculated by performing curve fitting with nonlinear least-squares. Elemental analysis was performed by ICP spectroscopy using a Shimadzu ICPS-7500 instrument. X-ray photoelectron spectra (XPS) were collected using a Thermo VG Sigma Probe X-ray photoelectron spectrometer with a Mg*K*α X-ray source (200 W). The base pressure both in the main and preparation chambers was equal to 3×10^{-9} mbar. All spectra were charge referenced to the C1*s* XPS peak (284.6 eV).

In order to evaluate the electrochemical performance of the material, composite electrodes were formed by mixing the active material with acetylene black and polytetrafuoroethylene (PTFE) in the weight ratio 85/10/5, and then pressing into pellets. The composite electrodes were dried at 120 °C in vacuum for 24 h before use. Button-type cells were assembled in a glove box filled with argon with less than 1 ppm H_2O and O_2. A cell was prepared by assembling the cathode, separator, and the anode in a sandwich structure. The anode was a lithium metal and the electrolyte was a 1 M solution of $LiClO_4$ in a mixture of EC/DEC in the volume ratio 1/1. The galvanostatic charge–discharge tests were carried out between 2.8 and 4.3 V (versus Li/Li^+) at a constant current density of 0.2 mA cm^{-2} (corresponding to the 0.07 C rate) using a LAND CT2001A cycle life tester.

3. Results and discussion

3.1. Structural study of LDHs precursor

The XRD pattern of the CoMn LDHs containing the interlayer CO_3^{2-} anion (Co/Mn = 2/1) is presented in Fig. 1 (30 °C). The phase crystallizes in the trigonal system (space group: *R*3*m*) with a basal spacing of 7.55 Å is similar to that of MgAl LDHs (CO_3) [24]. The peaks at about 29.7° and 33.4° (marked with*) in Fig. 1 (30 °C) are attributed to the characteristic reflections of $LiOH\cdot H_2O$ mixed with LDHs previously. During the coprecipitation, most Mn^{II} was oxidized to Mn^{III} by the oxygen in air. The structure of LDHs is based on stacked brucite-type $M(II)_x M(III)_{1-x}(OH)_2$ slabs, and the occupation of *M*(III) induced an excess of positive charge of the layer, which was balanced by CO_3^{2-} ions intercalated in the interslab space. Water molecules were also cointercalated between layers and participated in stabilizing the structure through their involvement in a hydrogen bonding network. The

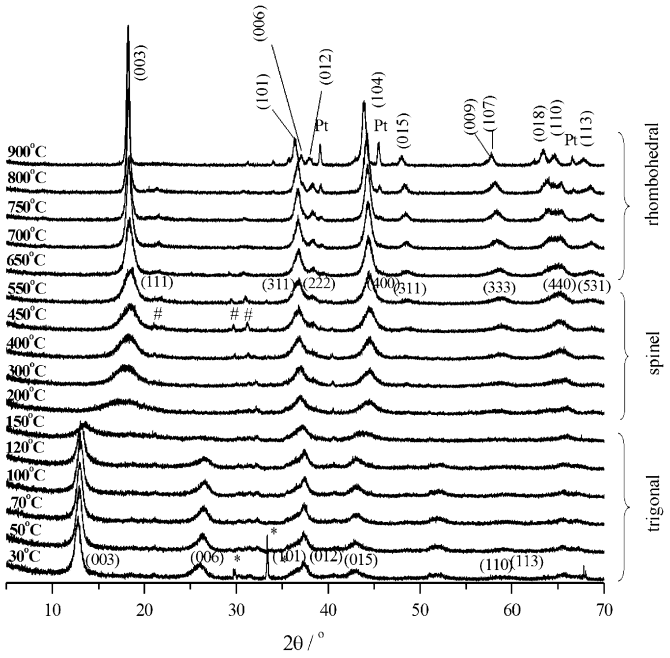

Fig. 1. *In situ* HT-XRD patterns of the mixture of CoMn LDHs and $LiOH \cdot H_2O$ in the temperature range 30–900 °C: *$LiOH \cdot H_2O$; #Li_2CO_3.

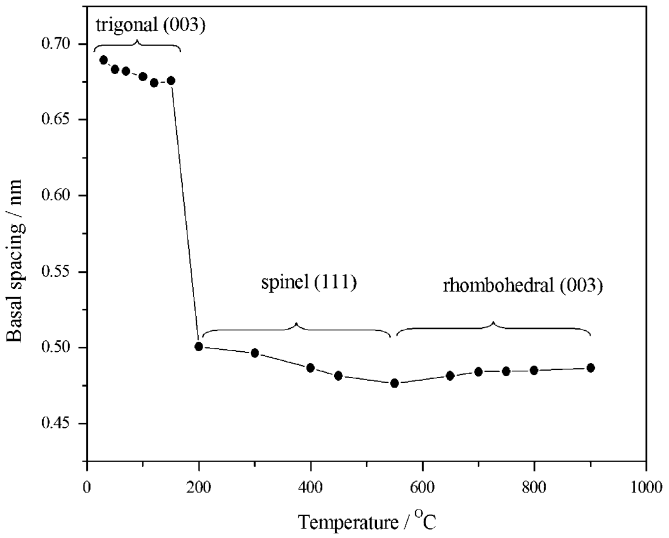

Fig. 2. The relationship between the interlayer basal spacing of the sample and temperature.

formula of $LDHs_{Co,\ Mn}(CO_3)$ (Co/Mn = 2/1) could be written as follows based on this work:

$$\underbrace{Co_{0.67}Mn_{0.33}(OH)_2}_{\text{slab}}\ \underbrace{(CO_3)_m(H_2O)_n}_{\text{interslab}}\ \underbrace{(H_2O)l}_{\text{adsorbed}}\ .$$

3.2. Thermal evolution monitored by in situ HT-XRD

A general view of the *in situ* HT-XRD patterns of the mixture of CoMn LDHs and $LiOH \cdot H_2O$ in the temperature range 30–900 °C as shown in Figs. 1 and 2 displays the variation of interlayer basal spacing of the CO_3^{2-} LDHs and the intermediate phase during the whole heat treatment process. It can be seen that there are three regions of interlayer spacing from 30 to 900 °C.

In the first range 30–150 °C, the successive XRD patterns exhibit a distinct change both in the reflection position and intensity, but no crystal transformation can be observed. As shown in Fig. 1, the (003) and (006) reflections of CO_3^{2-}LDHs moved to higher 2θ angle remarkably (d_{003} basal spacing decreased from 6.89 to 6.75 Å in Fig. 2), accompanied with a progressive decrease in the intensity. This is related to the extraction of the adsorbed and interlamellar water, which has been confirmed by other researchers in studying the thermal decomposition of LDHs materials [30].

When heated at 150–200 °C, a sharp fall of interlayer spacing value from 6.75 to 5.00 Å was observed. The structure of LDHs transformed to $Co[CoMn]O_4$ with a spinel structure rapidly, and the subsequent growth of a lithiated spinel phase was derived predominantly from $Co[CoMn]O_4$ intermediate product. The (003) peak of LDHs transformed to the (111) peak of the spinel, accompanied with the deintercalation of the remaining interlamellar water molecules and partial decomposition of the carbonate anions, as reported in the previous research work on the thermal decomposition of CO_3^{2-} LDHs [17,31–33]. In the following range, Li^+ was intercalated into the spinel lattice and thus the spinel crystal phase was reinforced, with the decrease in $d_{1\,1\,1}$ basal spacing of spinel from 5.00 Å at 200 °C to 4.76 Å at 550 °C. The XRD pattern is similar to that of LT-$LiCoO_2$ obtained at 400 °C by Shao-Horn et al. [12], which was indexed to the lithated-spinel $Li_2[Co_2]O_4$ structure.

As heated from 550 to 900 °C, the spinel structure became distorted and subsequent splitting of some spinel reflections was observed. The (222) reflection of spinel split into (006) and (012) reflections of the rhombohedral unit, while the (440) split into (108) and (110) reflections of rhombohedral unit. At about 750 °C, the layered phase was obtained and the spinel structure transformed to an α-$NaFeO_2$ crystal phase. The diffraction of the product can be indexed in rhombohedral system (space group:$R\bar{3}m$), similar to that of layered $LiCoO_2$. The interlayer spacing increased a little from 550 to 900 °C, which is related to the phase transformation and cell expansion. The reflection intensity of the layered structure became stronger as the temperature increased slowly to 900 °C. It should be noted that the peaks at about 39.1°, 45.5° and 66.5° (marked with Pt) are attributed to the characteristic reflections of platinum substrate used in the *in situ* HT-XRD experiment.

During the phase transformation, only a little change in the stacking sequence of oxygen atom layers occurs (from hexagonal close-packed to cubic close-packed, then to hexagonal close-packed), as a result the distance of oxygen layers represents the interlayer basal spacing of the material, i.e., the distance of (003) planes both in the trigonal system and rhombohedral system as well as (111) planes in the cubic system.

3.3. Thermal decomposition monitored by thermogravimetric (TG)–mass spectrometry (MS)

Simultaneous TG–differential thermal analysis (DTA) technique combined with MS analysis was found to be useful in the study of thermal behavior of the composites over a wide temperature range, and thus it was used to investigate the reaction process during the heat treatment of the mixture of CoMn LDHs and $LiOH \cdot H_2O$. As shown in Fig. 3, there are three marked weight loss stages in the TG curve in the temperature ranges 35–95, 300–550 and 550–800 °C, respectively. At the same time, three endothermic peaks were observed in the DTA curve at the temperatures of 74, 430 and 750 °C, accordingly. It should be noted that there was no distinguishable endothermic peak in the DTA curve corresponding to the gentle weight loss stage in the temperature range 95–300 °C.

During the temperature range 30–300 °C (the first two weight loss stages), two endothermic peaks were observed with the evolution of H_2O determined by MS. The first one at 120 °C is due to the loss of surface adsorbed and interlayer water in LDHs which has been confirmed by the shift of (003) reflection to higher angle 2θ by *in situ* HT-XRD (Fig. 1), as well as crystal water in $LiOH \cdot H_2O$. The water evolved at 180 °C is possibly associated with abruption of hydroxyl group from LDHs layers. As a result, the interlamellar distance presented a sharp decrease at 180 °C and the trigonal (003) peak transformed to spinel (111) peak with higher angle values (as shown in Fig. 1).

In the third loss event (300–550 °C), there was an endothermic peak at about 430 °C accompanied by the evolution of H_2O at 457 °C. It should be noted that the characteristic reflections of Li_2CO_3 were observed at 450 °C in Fig. 1 (marked with #), which results from the reaction between CO_3^{2-} and LiOH. The evolution of H_2O detected by MS was another product of this reaction. Meanwhile, Li^+ inserted into the lattice of the host, and thus the lithiated-spinel structure was developed in the temperature range 300–550 °C. From 550 to 800 °C, there was a weight loss related to CO_2 evolution as a result of the decomposition of Li_2CO_3, which produced during the formation of spinel structure. CO_2 signal was detected by MS at 600–800 °C, much higher than that of the pure CO_3^{2-} LDHs phase occurring at 300–550 °C [26,34]. In this event, the weight loss was associated with the intercalation of Li^+ into the spinel lattice, and thus the structure distortion and transformation to layered rhombohedral phase. This is consistent with the results of *in situ* HT-XRD.

3.4. Structure and composition of the layered $Li[Co_xMn_{1-x}]O_2$

The powder XRD patterns of $Li[Co_xMn_{1-x}]O_2$ with different Co/Mn ratio are shown in Fig. 4, which can be indexed on the basis of the α-$NaFeO_2$ type structure. The layered phase crystallizes in the rhombohedral system, space group $R\bar{3}m$ with an interlayer spacing close to 4.67 Å. The lattice parameters of $Li[Co_xMn_{1-x}]O_2$ calculated from the XRD patterns are listed in Table 1. Increase of Co content results in the expansion of the unit cell parameters slightly. It has been reported that large c/a ratio suggests a well-defined layered structure [4], so the c/a ratios close to 5 indicate a well-defined layered structure and high cation ordering in this work.

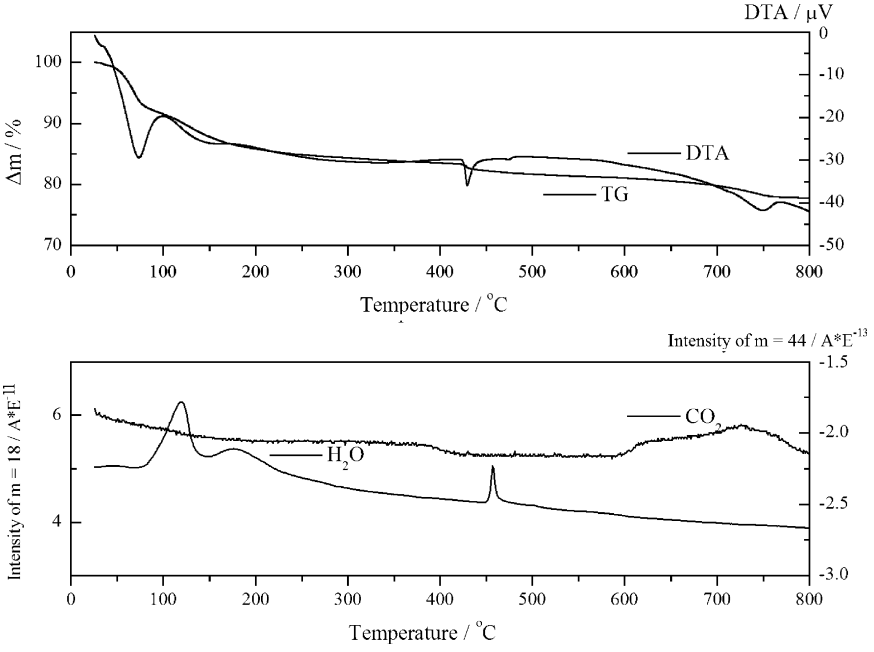

Fig. 3. Thermogravimetry (TG), differential thermal analysis (DTA) and evolved gas analysis (H_2O and CO_2) results of the mixture of CoMn LDHs and $LiOH \cdot H_2O$ measured in nitrogen.

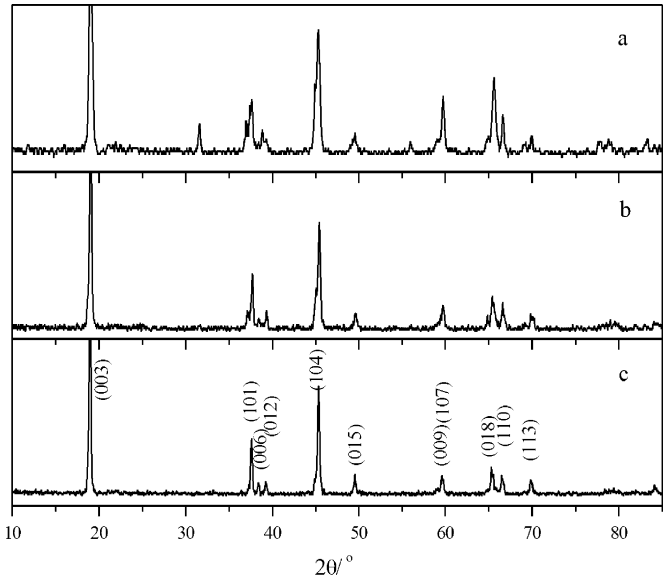

Fig. 4. Powder XRD patterns of $Li[Co_xMn_{1-x}]O_2$: (a) $x = 0.67$; (b) $x = 0.75$; and (c): $x = 0.80$.

Table 1
Lattice parameters of samples $Li[Co_xMn_{1-x}]O_2$ with different Co/Mn ratio

Input ratio of Co/Mn	a (Å)	c (Å)	c/a
2/1	2.80±0.01	13.97±0.01	4.99
3/1	2.80±0.01	13.98±0.01	4.99
4/1	2.81±0.01	14.02±0.01	4.99

Fig. 5(a) shows the Fourier transform modulus $F(R)$ spectra of the EXAFS at the Co and Mn K-edges, while Fig. 5(b) displays the experimental (solid line) and fitting (dot line) k-space data of Co–O and Mn–O coordination. The fitting parameters are listed in Table 2. The $F(R)$ modulus of the EXAFS signal is a pseudo-radial distribution function around the absorber atoms. The different peaks can be associated to various neighbor shells and the positions of the peak maxima are linked to the bonding lengths (uncorrected from the backscattering phase shift at this stage). At the Co and Mn K-edges (Fig. 5), the $F(R)$ spectra present the same main characteristics. The $F(R)$ modulus at Co K-edge is close to that of literature [35]: the first peak located around 1.4 Å corresponds undoubtedly to the first oxygen neighbors; the second peak at about 2.3 Å corresponds to the second (transitional metal) shell, which can be attributed to Co–Co second nearest neighbors and eventually to Co–Mn distances. Data analysis revealed the Co–O distance of 1.94 Å with CN of 5.5 for $Li[Co_{0.80}Mn_{0.20}]O_2$, and the Mn–O distance of 1.91 Å with CN of 5.4. The rather close parameters of Co and Mn indicate that the local octahedral environments of the transitional metals in this material are similar to each other.

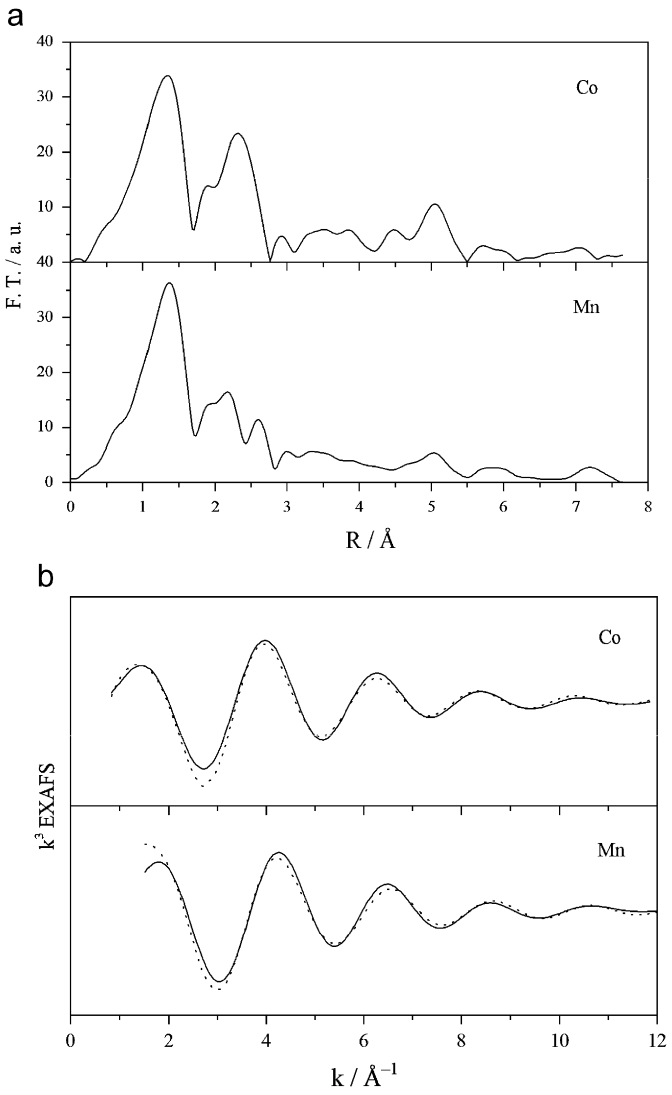

Fig. 5. (a) Fourier transforms of Co and Mn K-edges EXAFS of $Li[Co_{0.80}Mn_{0.20}]O_2$ and (b) Experimental (solid line) and fitting (dot line) EXAFS curves with k^1-weight of Co–O and Mn–O coordination in $Li[Co_{0.80}Mn_{0.20}]O_2$.

Table 2
EXAFS results for $Li[Co_{0.80}Mn_{0.20}]O_2$

	CN	R (Å)	σ^2 (10^{-3} Å^2)	R_f (%)
Co–O	5.5±0.2	1.94±0.01	3.0±0.2	18.6
Mn–O	5.4±0.2	1.91±0.01	3.0±0.2	19.4

Note: CN is the coordination number; R the interatomic distance; σ the Debye–Waller factor; R_f is a measure of the agreement between experimental and theoretical EXAFS curves. $R_f < 20\%$ indicates a very good fit. The precision of CN is estimated to be $\leqslant 20\%$.

Elemental analysis of the products performed by ICP spectroscopy is listed in Table 3. The results show that the Co/Mn molar ratio in $Li[Co_xMn_{1-x}]O_2$ was near to the input ratio, while lithium content increased as the x changed from 0.67 to 0.80. This might be related to the existence of amorphous oxides in the sample with lower Co

Table 3
Chemical compositions of $Li[Co_xMn_{1-x}]O_2$

Input ratio of Co/Mn	Elemental content			Molecular formula
	Li (wt%)	Mn (wt%)	Co (wt%)	
2/1	8.03±0.01	23.41±0.01	51.67±0.01	$Li_{0.89}[Co_{0.67}Mn_{0.33}]O_2 \cdot 0.72H_2O$
3/1	8.70±0.01	18.10±0.01	58.55±0.01	$Li_{0.95}[Co_{0.75}Mn_{0.25}]O_2 \cdot 0.61H_2O$
4/1	9.48±0.01	13.97±0.01	59.47±0.01	$Li_{1.02}[Co_{0.81}Mn_{0.19}]O_2 \cdot 0.71H_2O$

The contents of cations were determined by ICP; the water content was calculated by TG.

content, such as MnO_2. As $x = 0.80$, single layered phase allows more Li^+ ions to be intercalated; moreover, the adsorption of small amount of lithium on the surface of the material leads to its higher content (Table 3). It is reported that a native surface film, mainly composed of Li_2CO_3, already exists on all transitional metal oxide cathode materials based on manganese, cobalt, and nickel [36]. This surface component could arise from the precursors used to synthesize these metal oxides or, more likely, from the reaction between the metal oxides and the CO_2 in the atmosphere during the processing of these strongly oxidizing materials [36].

X-ray photoelectron spectroscopy (XPS) can provide chemical information such as the oxidation state, as well as the semi-quantitative composition of the surface, and is thus a very useful method for studying the surface properties. Fig. 6 displays the XPS results for $Li[Co_{0.80}Mn_{0.20}]O_2$. The binding energy of $Mn2p_{3/2}$ is 642.8 eV is in agreement with that of MnO_2 in the literature [37], indicating that the predominant Mn species near the surface is Mn^{IV}. According to the rule that compounds containing high-spin Co^{II} ions have strong shake-up peaks in Co2*p* spectra of XPS, while Co^{III} is diamagnetic and has no satellite peak [38], valence of cobalt can be determined by the XPS spectroscopy. The $Co2p_{3/2}$ and $Co2p_{1/2}$ peaks in Fig. 6 at 780.4 and 795.5 eV respectively, are close to those of $ZnCo_2O_4$ reported previously [39]. No visible satellite peaks can be observed, indicating that most of Co^{II} was oxidated to Co^{III} during the solid reaction. The O1*s* spectroscopy contains two oxygen contributions: component one at 529.8 eV is typical of metal–oxygen bonding; the other at 531.5 eV is usually associated with oxygen in OH^- groups. The presence of this contribution in the O1s spectroscopy indicates that the surface of the materials was hydroxylated to some extent.

Electrochemical performance of $Li[Co_xMn_{1-x}]O_2$

The charge–discharge curves of the cell for the first cycle with the samples a, b and c used as cathode materials are illustrated in Fig. 7, and the cycling behavior is shown in Fig. 8. The three samples have an initial EMF of 3.2–3.3 V. It can be seen in Fig. 7 that the molar ratio of Co/Mn has a significant influence on the charge–discharge capacity. The first charge and discharge capacities of sample a ($Li[Co_{0.67}Mn_{0.33}]O_2$) are 45.5 and 43.4 mAh g^{-1}, respectively. The specific capacity of sample a after the 15th cycle maintains at 40.6 mAh g^{-1} with very little decay capacity (Fig. 8). The capacity of the material was improved with the increase of Co/Mn ratio, and the reversible capacity of sample b is 60.8 mAh g^{-1}, while sample c ($Li[Co_{0.80}Mn_{0.20}]O_2$) presents the highest reversible capacity of 122.5 mAh g^{-1} (Fig. 8), indicating that higher content of Co is favorable for the intercalation–deintercalation of lithium ions. The capacity of sample c decays slowly with repeated cycling and the retained specific capacity after the 15th cycle is 102.6 mAh g^{-1}, which indicates a viable stable cycling behavior with high coulombic efficiency.

Based on the results of structural characterization, it can be concluded that the higher content of Co prevents the formation of the spinel phase and leads to a well-defined layered structure with advantages of higher theoretical capacity, easier intercalation of Li^+, and thus a higher reversible capacity. On the other hand, the mean valence of Mn^{IV} indicates an inert electrochemical property of Mn, and the cathode reaction occurs primarily on the redox of cobalt. Consequently, the reversible capacity was improved as the Co/Mn ratio increased. Of the three materials with different Co/Mn molar ratio, $Li[Co_{0.80}Mn_{0.20}]O_2$ possesses a single layered phase and relatively promising lithium insertion properties, with a specific capacity of 122.5 mAh g^{-1} and rather stable cycling behavior.

4. Conclusions

Layered $Li[Co_xMn_{1-x}]O_2$ was synthesized by solid-state reaction of the precursor CoMn LDHs and LiOH. Firstly, an intermediate phase with spinel structure appeared between 200 and 550 °C, then Li^+ was intercalated into the lattice of spinel, and thus led to the structure distortion and transformation from a lithiated spinel phase to layered rhombohedral $Li[Co_xMn_{1-x}]O_2$ with α-$NaFeO_2$ structure. EXAFS results indicated that the local environment of the transitional metals are similar in $Li[Co_xMn_{1-x}]O_2$. XRD patterns and ICP results demonstrated that the crystal integrity and the capacity of lithium intercalation were improved along with the increase in Co/Mn molar ratio. XPS determination revealed that Mn^{IV} and Co^{III} predominate near the surface of the sample. The electrochemical behavior of $Li[Co_{0.80}Mn_{0.20}]O_2$ as a cathode material in lithium secondary batteries showed

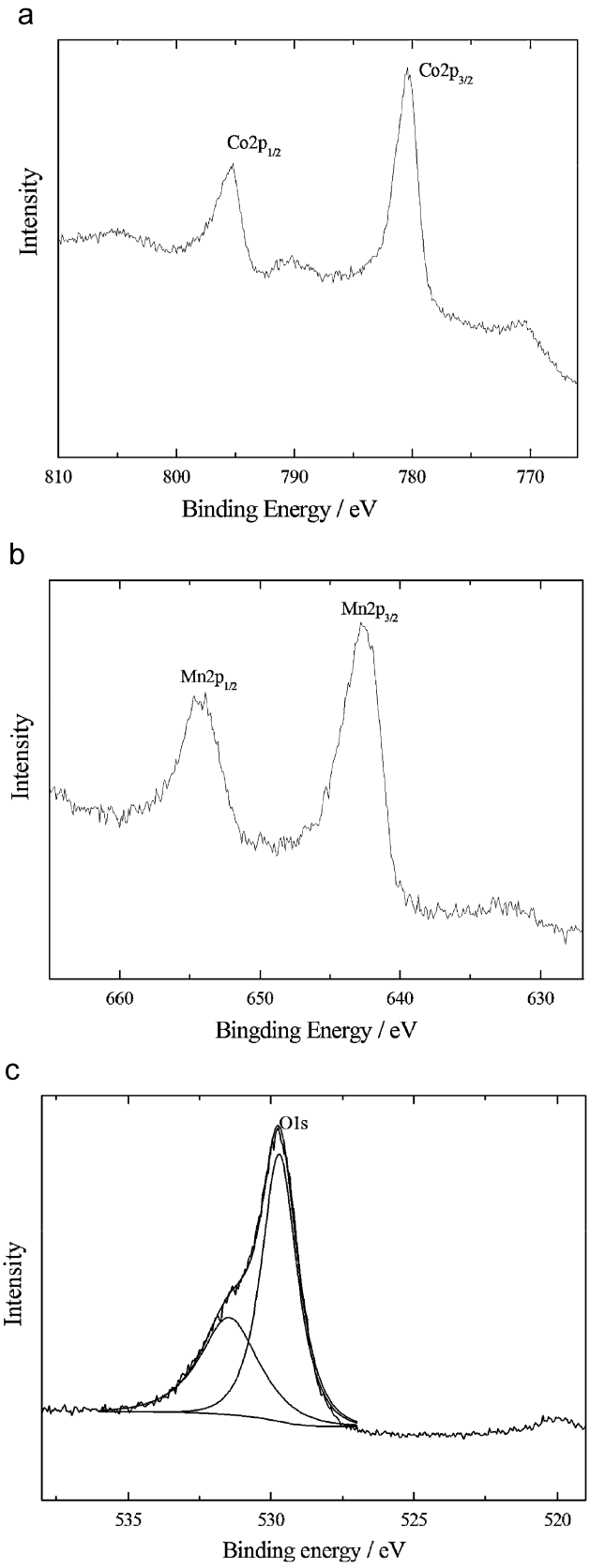

Fig. 6. X-ray photoelectron spectra of Co, Mn and O in $Li[Co_{0.80}Mn_{0.20}]O_2$: (a) Co; (b) Mn; and (c) O.

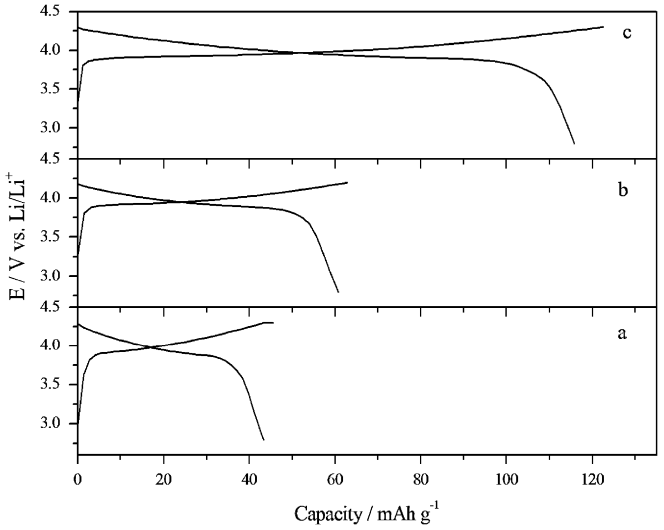

Fig. 7. Charge–discharge curves of $Li[Co_xMn_{1-x}]O_2$ as cathode material for the first cycle: (a) $x = 0.67$; (b) $x = 0.75$; and (c) $x = 0.80$.

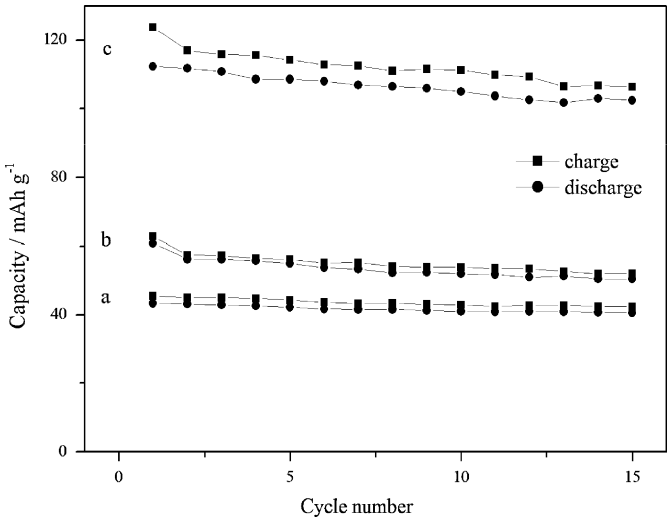

Fig. 8. Charge–discharge capacities of $Li[Co_xMn_{1-x}]O_2$ on cycling: (a) $x = 0.67$; (b) $x = 0.75$; and (c) $x = 0.80$.

that this material exhibits high charge–discharge capacities of over 120 mAh g^{-1} between 2.8 and 4.3 V and viable cycling stability.

Acknowledgments

This project was supported by the National Natural Science Foundation Major International Joint Research Program (Grant no.: 20620130108), National Natural Science Foundation of China (Grant nos.: 20601001 and 50503001), the Program for New Century Excellent Talents in University (Grant nos.: NCET-05-121 and NCET-05-0204) and the 111 Project (Grant no.: B07004). Program for Changjiang Scholars and Innovative Research Team in University (PCSIRT) in China. We also acknowledge Beijing Synchrotron Radiation Facility (BSRF) for

provision of synchrotron radiation facilities and thank Dr. Yaning Xie and Tao Liu for assistance in using beamline 4W1B.

References

[1] F. Zhang, K. Ngala, M.S. Whittingham, Electrochem. Commun. 2 (2000) 445–447.
[2] F. Lecas, S. Rohs, M. Anne, P. Strobel, J. Power Sources 54 (1995) 319–322.
[3] M.S. Whittingham, R. Chen, T. Chirayil, P. Zavalij, Electrochem. Soc. Proc. 96-5 (1996) 76–85.
[4] A.R. Armstrong, A.D. Robertson, P.G. Bruce, Electrochim. Acta 45 (1999) 285–294.
[5] A.R. Armstrong, P.G. Bruce, Nature 381 (1996) 499–500.
[6] J.M. Paulsen, C.L. Thomas, J.R. Dahn, J. Electrochem. Soc. 146 (1999) 3560–3565.
[7] Z. Lu, D.D. Macneil, J.R. Dahn, Electrochem. Solid State Lett. 4 (2001) A191–A194.
[8] X. Yang, J. McBeen, W. Yoon, C.P. Grey, Electrochem. Commun. 4 (2002) 649–654.
[9] K.M. Shaju, G.V. Subba Rao, B.V.R. Chowdari, Electrochim. Acta 48 (2003) 1505–1514.
[10] K.M. Shaju, G.V. Subba Rao, B.V.R. Chowdari, Electrochim. Acta 48 (2003) 2691–2703.
[11] K. Numata, S. Yamanaka, Solid State Ion. 118 (1999) 117–120.
[12] Y. Shao-Horn, S.A. Hackney, A.J. Kahaian, M.M. Thackeray, J. Solid State Chem. 168 (2002) 60–68.
[13] K.M. Shaju, G.V. Subba Rao, B.V.R. Chowdari, Solid State Ion. 152–153 (2002) 69–81.
[14] A. Caballero, L. Hernán, J. Morales, E. Rodríguez Castellón, J. Santos, J. Power Sources 128 (2004) 286–291.
[15] S.B. Jang, S.-H. Kang, K. Amine, Y.C. Bae, Y.-K. Sun, Electrochim. Acta 50 (2005) 4168–4173.
[16] L. Zhang, H. Noguchi, M. Yoshio, J. Power Sources 110 (2002) 57–64.
[17] B.L. Cishing, J.B. Goodenough, Solid State Sci. 4 (2002) 1487–1493.
[18] C. Vaysse, L. Guerlou-Demourgues, C. Delmas, Inorg. Chem. 41 (2002) 6905–6913.
[19] F. Canavi, F. Trifiro, A. Vaccari, Catal. Today 11 (1991) 173–301.
[20] A. Vaccari, Catal. Today 41 (1998) 53–71.
[21] K.S. Han, L. Guerlou-Demourgues, C. Delmas, Solid State Ion. 98 (1997) 85–92.
[22] W. Jones, M. Chibwe, in: I.V. Mitchell (Ed.), Pillared Latered Structures, Elsevier, London, 1990 p. 67.
[23] S. Miyata, A. Okada, Clays Clay Miner. 25 (1977) 14.
[24] A. Trave, A. Selloni, A. Goursot, D. Tichit, J. Weber, J. Phys. Chem. B 106 (2002) 12291.
[25] P.J. Dunn, D.R. Peacor, T.D. Palmer, Am. Miner. 64 (1979) 127–130.
[26] F. Kovanda, T. Grygar, V. Dorničák, Solid State Sci. 5 (2003) 1019–1026.
[27] K. Chibwe, W. Jones, J. Chem. Soc. Chem. Commun. (1989) 926.
[28] R.L. Goswamee, P. Sengupta, K.G. Bhattacharyya, Di.K. Dutta, Appl. Clay Sci. 13 (1998) 21–34.
[29] Z.P. Xu, H.C. Zeng, Chem. Mater. 13 (2001) 4564–4572.
[30] M. Wei, Q. Yuan, D.G. Evans, Z. Wang, X. Duan, J. Mater. Chem. 15 (2005) 1197–1203.
[31] T. Stanimirova, I. Vergilov, G. Kirov, N. Petrova, J. Mater. Sci. 34 (1999) 4153–4161.
[32] F. Millange, R.I. Walton, D. O'Hare, J. Mater. Chem. 10 (2000) 1713–1720.
[33] T. Moroz, L. Razvorotneva, T. Grigorieva, M. Mazurov, D. Arkhipenko, V. Progov, Appl. Clay Sci. 18 (2001) 29–36.
[34] S. Carlino, M.J. Hudson, Solid State Ion. 110 (1998) 153–161.
[35] M. Holzapfel, O. Proux, P. Strobel, C. Darie, M. Borowski, M. Morcrette, J. Mater. Chem. 14 (2004) 102–110.
[36] D. Aurbach, J. Power Sources 89 (2000) 206–218.
[37] V.R. Galakhov, M.A. Korotin, N.A. Ovechkina, E.Z. Kurmaev, V.S. Gorshkov, D.G. Kellerman, Eur. Phys. J. B 14 (2000) 281–286.
[38] G. Hu, L. He, Chin. J. Anal. Chem. 29 (2001) 1431–1433.
[39] M. Oku, K. Hirokawa, J. Elect. Spectrosc. 8 (1976) 475–481.